Electronic Supplementary Material (ESI) for Dalton Transactions.

Fluoride anion complexation and transport using a stibonium cation stabilized by an intramolecular P=O→Sb pnictogen bond

Vanessa M. Gonzalez, Gyeongjin Park, Mengxi Yang, François P. Gabbaï*

Department of Chemistry, Texas A&M University, College Station, Texas 77843-3255, USA

SUPPORTING INFORMATION

Synthetic details

General considerations: [**1**]Br[1] and [Ph_4Sb]OTf[2] were prepared by following procedures available in the literature. KF, triphenylphosphine oxide, and $NOBF_4$ were purchased from Alfa Aesar. High purity grade 4-(2-Hydroxyethyl)piperazine-1-ethanesulfonic acid (HEPES) was purchased from VWR Life Science. 1-Palmitoyl-2-oleoyl-sn-glycero-3-phosphocholine (POPC) was purchased from Avanti Polar Lipids. Valinomycin was purchased from BioWorld. Potassium gluconate was purchased from TCI America. Na_2SO_4 was purchased from EM Science. All commercially available compounds were used as received. The Mini-Extruder used for size selection of the vesicles was purchased from Avanti Polar Lipids. The Sephadex G-50 column was purchased from GE Healthcare – Life Sciences. All solvents were ACS reagent grade and used as received. ^{1}H, ^{13}C, ^{19}F NMR, ^{31}P NMR spectra were recorded at room temperature on a Varian Inova 500 FT NMR spectrometer, a Bruker Avance 500 NMR spectrometer or a Bruker Ascend 400 NMR spectrometer. ^{1}H and ^{13}C NMR chemical shifts are given in ppm and are referenced to residual ^{1}H and ^{13}C solvent signals, respectively. The ^{19}F NMR chemical shifts are referenced to $CFCl_3$. The ^{31}P NMR chemical shifts are referenced to H_3PO_4. Mass spectrometry analyses were performed in-house at the Center for Mass Spectrometry. Elemental analyses were performed by Atlantic Microlab (Norcross, GA). ISE assays were performed with a Thermo Scientific Orion 9609BNWP Fluoride Ion Selective Electrode connected to a pH-meter giving readings in mV (PHM 290, Meter lab, Radiometer Analytical S.A., Villeurbanne, Cedex, France). Tetrahydrofuran will be abbreviated as THF.

Crystallographic measurements. The crystallographic measurements were performed at 110 K using a Bruker D8 Venture (Cu-Kα radiation, λ = 1.54178 Å) or a Brucker D8 QUEST diffractometer (Mo-Kα radiation, λ = 0.71069 Å) equipped with Photon III detectors. In each case, a specimen of suitable size and quality was selected and mounted onto a nylon loop. Integrated intensity information for each reflection was obtained by reduction of the data frames with the program APEX3.[3] The semiempirical method SADABS was applied for the absorption correction.[4] The structures were solved by direct methods (ShelXT)[5] or intrinsic phasing and refined by the full-matrix least-squares technique against F^2 with anisotropic temperature parameters for all non-hydrogen atoms (ShelXL)[6] using Olex2 interface.[7] The hydrogen atoms were placed in calculated positions and refined using a riding model approximation. Diamond4 was employed for the final data presentation and structure plots. The data has been deposited with the Cambridge Structural Database. CCDC 2106460-2106461 contains the supplementary crystallographic data for this paper**.**

Synthesis of [*o*-$Ph_2P(=O)(C_6H_4)SbPh_3$][BF_4] ([2]BF_4): This experiment was performed under ambient conditions. In a 20 mL vial, [**1**]Br (53.4 mg, 0.0769 mmol) was dissolved in 5 mL of "as-provided" CH_2Cl_2 and 0.5 mL of water was added to the solution. Upon addition of $NOBF_4$ (13.8 mg, 0.118 mmol), the solution turned to a light-yellow color. The resulting mixture was stirred vigorously for 30 minutes after which the aqueous phase was extracted with CH_2Cl_2 (2 x 5 mL)

and water (5 mL). The combined organic phases were dried over Na_2SO_4 and the solvent was removed under vacuum to afford a yellow solid. The solid was dissolved in CH_2Cl_2 (1 mL) and precipitated by addition of Et_2O (10 mL). The resulting white solid was collected via filtration and dried under vacuum to afford 50.4 mg of product (91% yield). Single crystals of [**2**]BF_4 were obtained as colorless blocks by vapor diffusion of Et_2O into a saturated $CDCl_3$ solution of the salt. ^{1}H NMR (500.13 MHz, $CDCl_3$) δ 8.12-8.05 (m, 1H), 8.05-7.98 (m, 1H), 7.89-7.82 (triplet, J = 5.90 Hz, 1H), 7.70-7.58 (m, 6H), 7.57-7.39 (m, 20H). ^{13}C NMR (125.77 MHz, $CDCl_3$, see Figure S2 for atom numbering) δ 137.25 (d, $J_{C\text{-}P}$ = 11.17 Hz, C_1 or C_{10}), 135.03 (s, C_2), 134.98 (s, C_3), 134.85 (d, $J_{C\text{-}P}$ = 11.34 Hz, C_4), 134.31 (d, $J_{C\text{-}P}$ = 11.48 Hz, C_5), 134.07 (d, $J_{C\text{-}P}$ = 2.78 Hz, C_6), 132.56 (d, $J_{C\text{-}P}$ = 99.76 Hz, C_7), 132.23 (s, C_8), 132.22 (d, $J_{C\text{-}P}$ = 11.15 Hz, C_9), 130.88 (d, $J_{C\text{-}P}$ = 8.03 Hz, C_1 or C_{10}), 130.57 (s, C_{11}), 130.34 (s, C_{12}), 129.52 (d, $J_{C\text{-}P}$ = 13.18 Hz, C_{13}), 127.12 (d, $J_{C\text{-}P}$ = 107.79 Hz, C_{14}). ^{31}P{^{1}H} NMR (161.95 MHz, $CDCl_3$) δ 31.33 (s). ESI-MS calcd for $C_{36}H_{29}OPSb^+$ $[M]^+$ 629.09887, found 629.0975. Elemental Analysis calculated (%) $C_{36}H_{29}POSbBF_4$: C, 60.29; H, 4.08; found C, 60.05; H, 4.16.

Synthesis of *o*-$Ph_2P(=O)(C_6H_4)SbFPh_3$ (2-F): This experiment was performed under ambient conditions. In a small vial, [**2**]BF_4 (15 mg, 0.021 mmol, 1 eq.) was dissolved in 2 mL of MeOH. An excess of KF (30 mg, 0.51 mmol, 24 eq.) was added to the MeOH solution and stirred for 30 minutes during which a white precipitate progressively formed. The precipitate was recovered by filtration and washed with MeOH to yield 5.2 mg of the product as a white powder (38% yield). Single-crystals of **2**-F were obtained as colorless needles by diffusion of Et_2O into a CH_2Cl_2 solution. ^{1}H NMR (500.13 MHz, CD_2Cl_2) δ 7.85-7.11 (broad, m). The product was hardly soluble in any solvent. Despite our best efforts, ^{13}C NMR could not be obtained because of its poor solubility. ^{19}F NMR (376.53 MHz, CD_2Cl_2) δ -61.10 (s). ^{31}P{^{1}H} NMR (162.00 MHz, CD_2Cl_2) δ 26.87 (s). Elemental Analysis calculated (%) $C_{36}H_{29}POSbF$: 66.59; H, 4.50; found C, 66.28; H, 4.79.

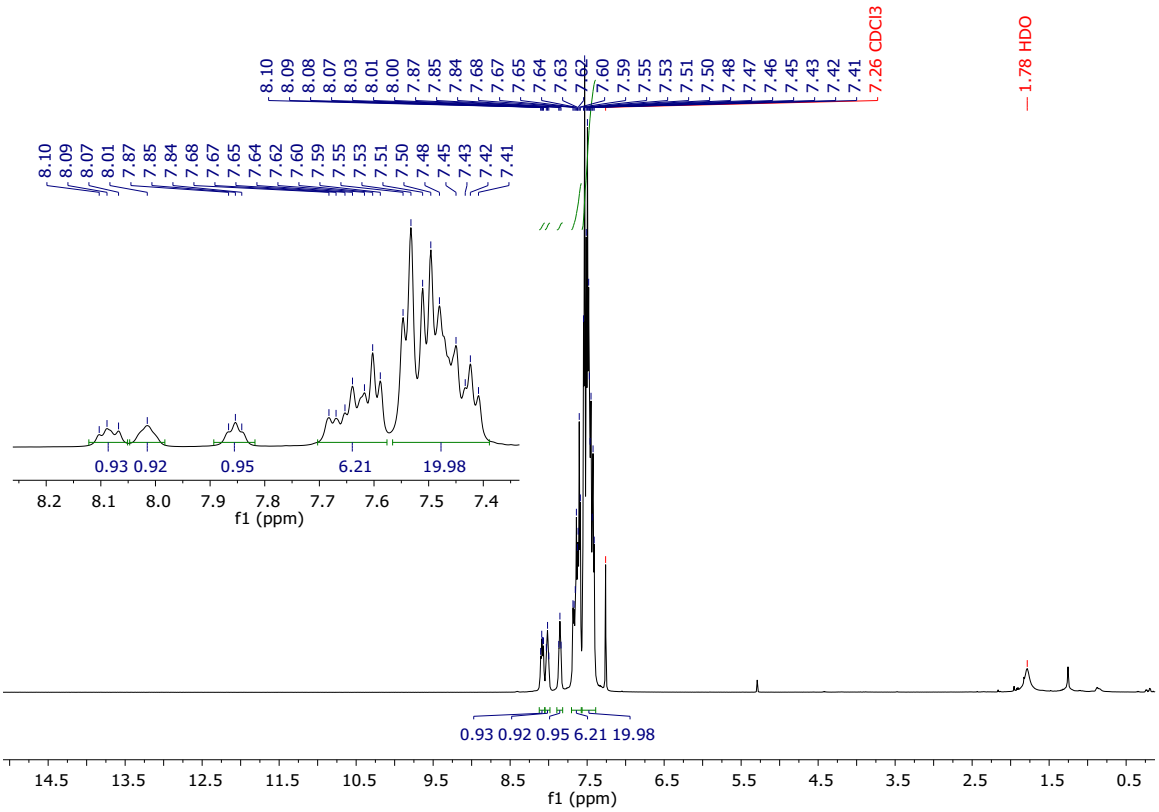

Figure S1. ^{1}H NMR spectrum of [**2**]BF_4 in $CDCl_3$.

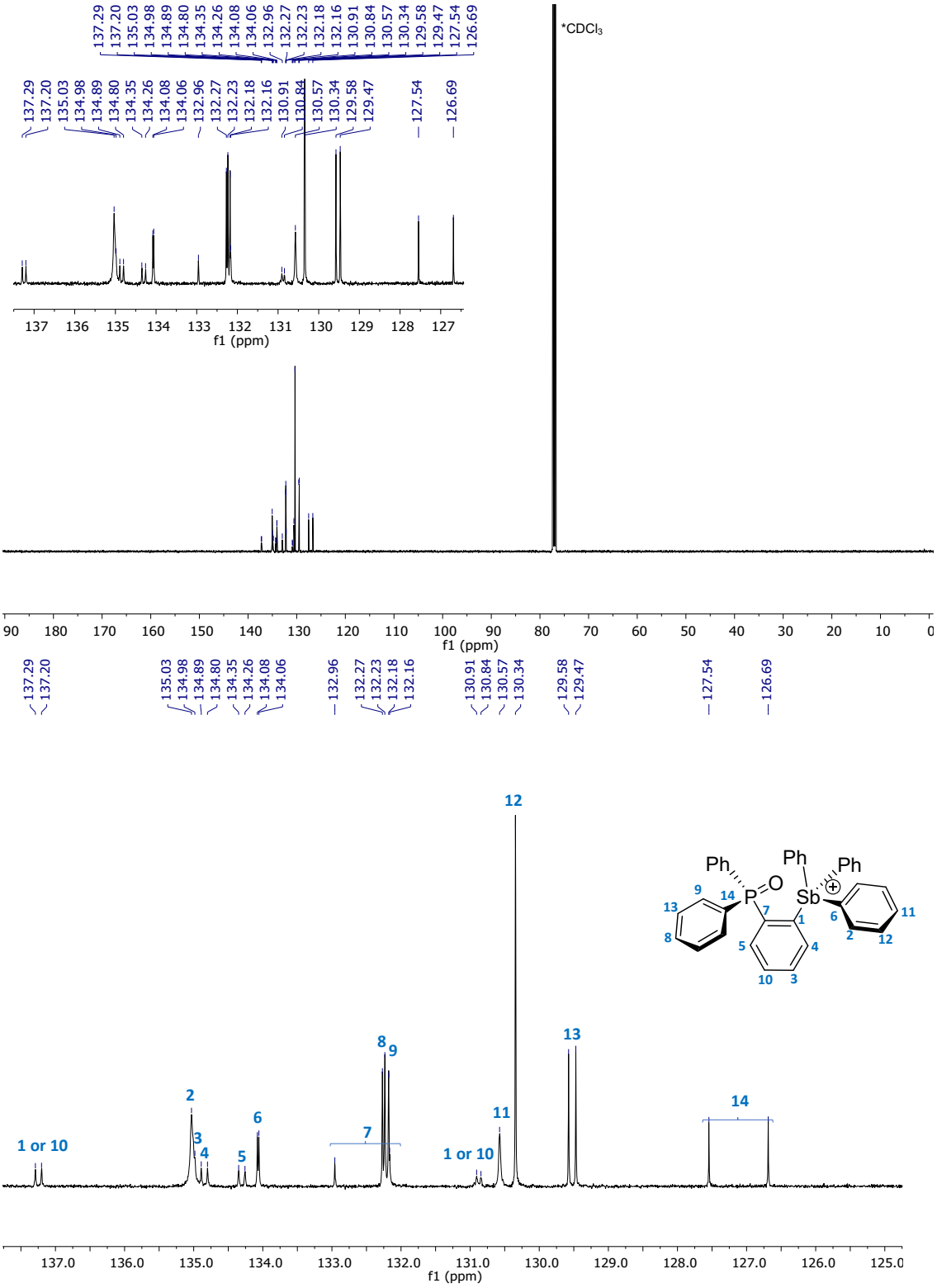

Figure S2. ^{13}C NMR spectrum of [**2**]BF_4 in $CDCl_3$.

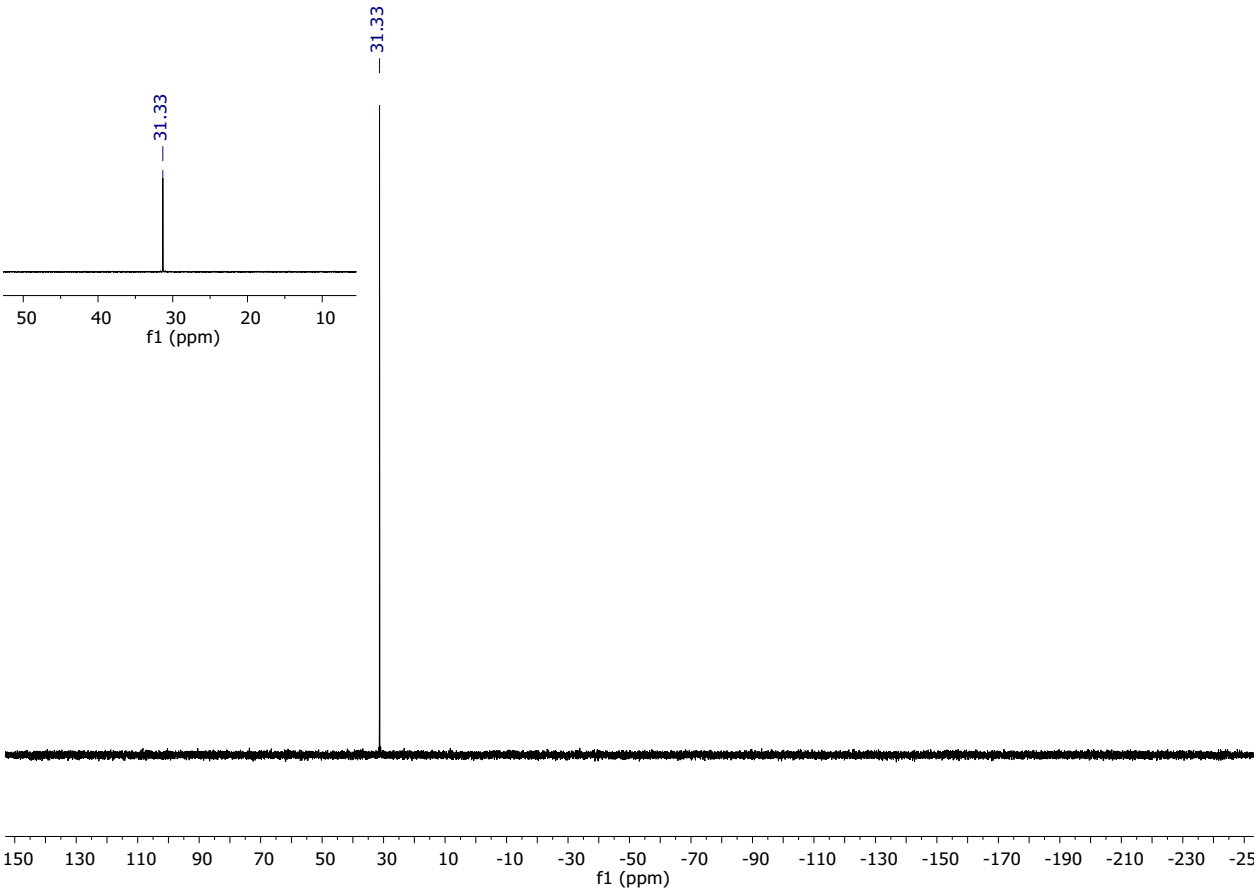

Figure S3. ^{31}P NMR spectrum of [**2**]BF_4 in $CDCl_3$.

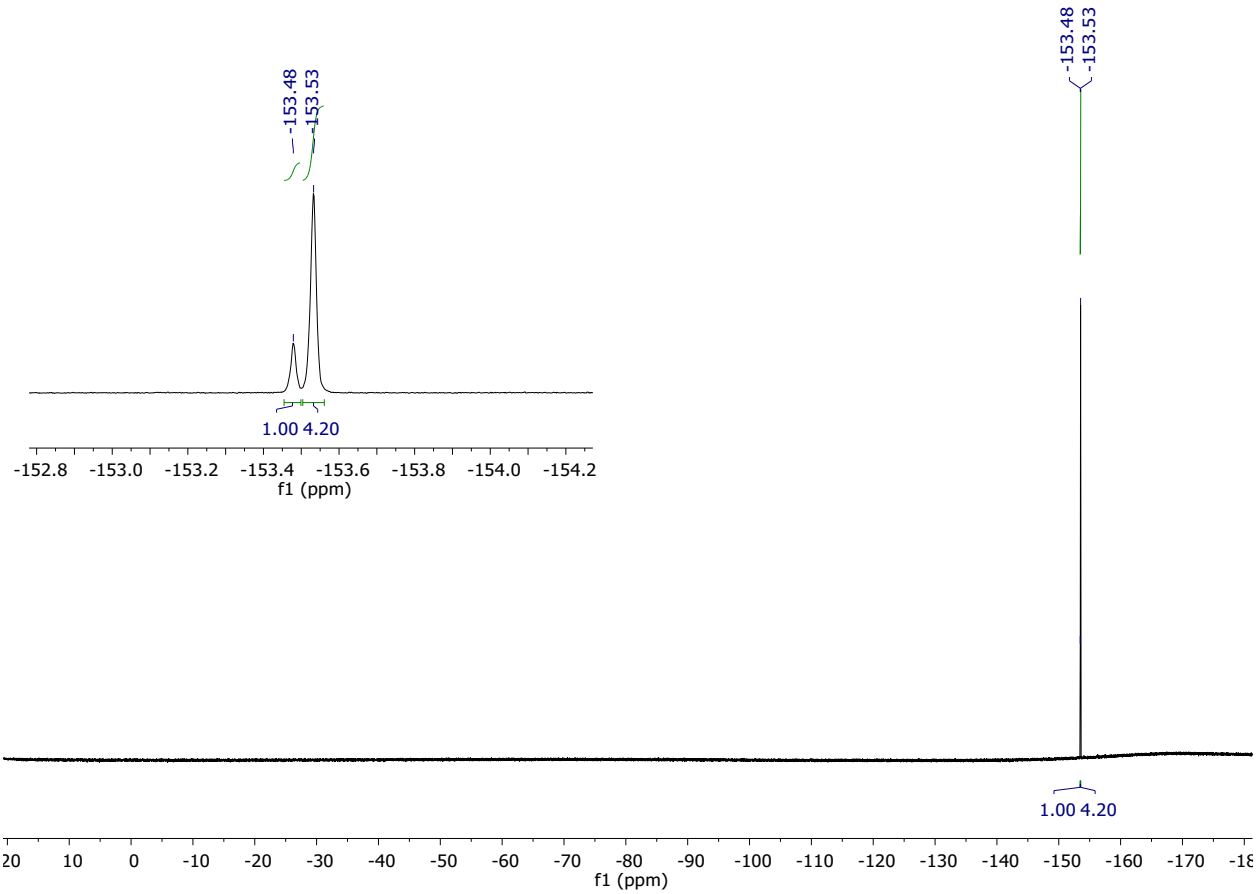

Figure S4. ^{19}F NMR spectrum of [**2**]BF_4 in $CDCl_3$.

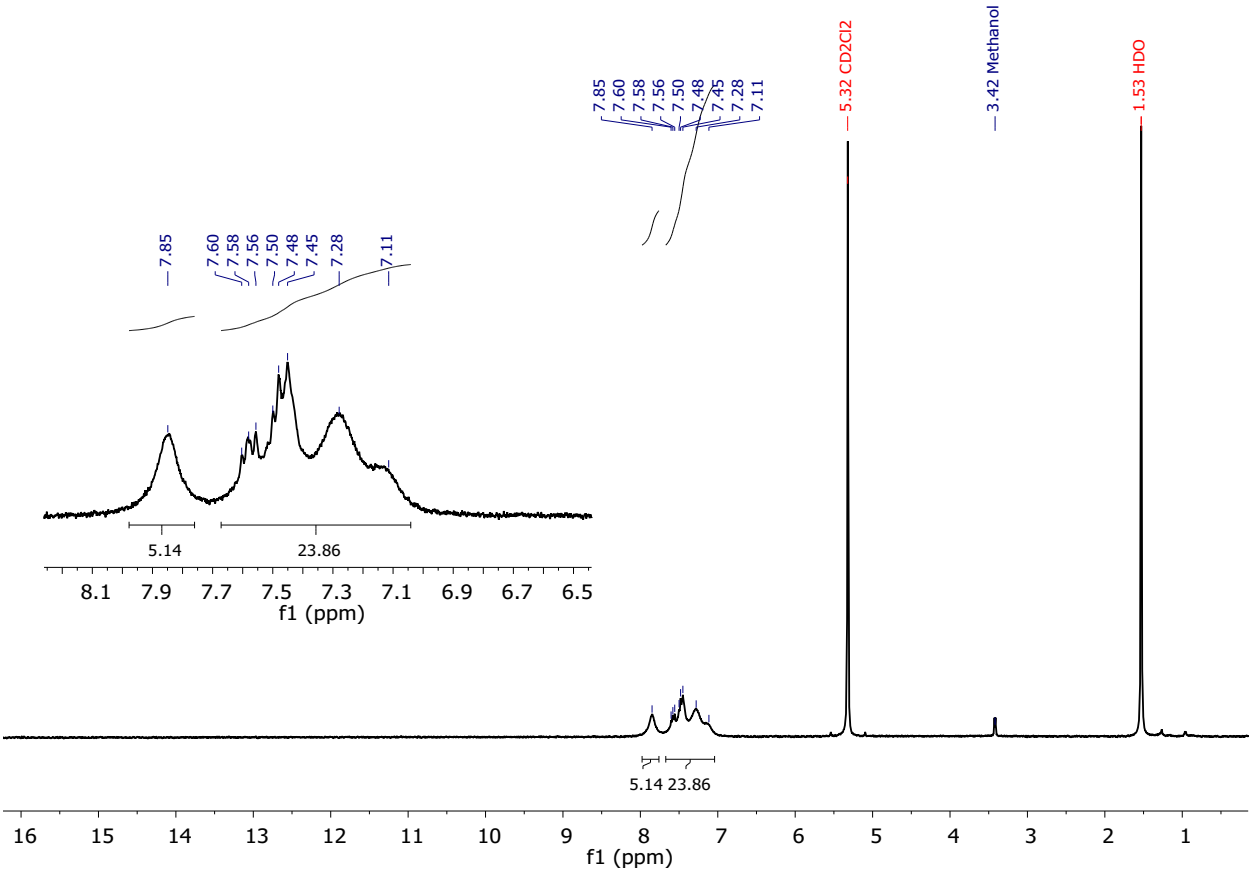

Figure S5. ^{1}H NMR spectrum of **2**-F in CD_2Cl_2.

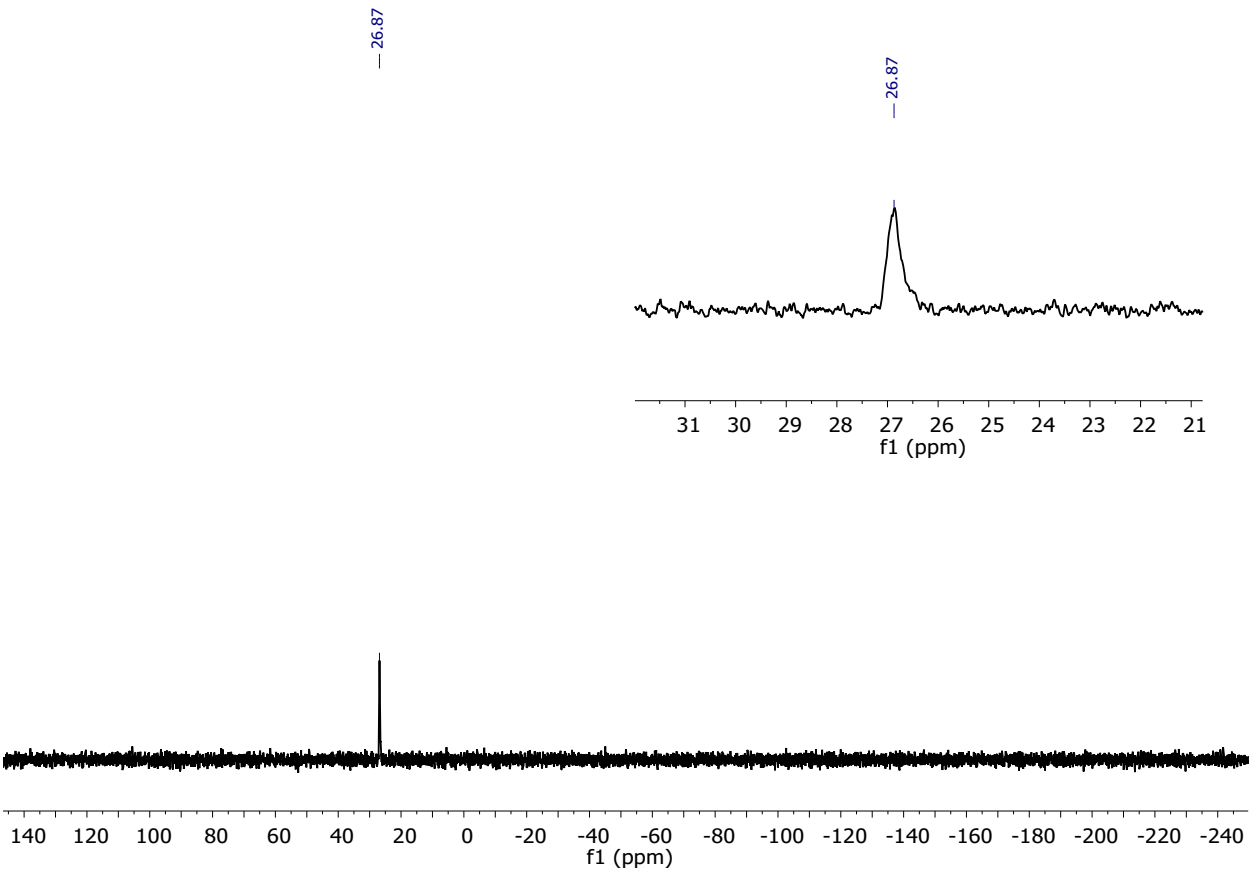

Figure S6. ^{31}P NMR spectrum of **2**-F in CD_2Cl_2.

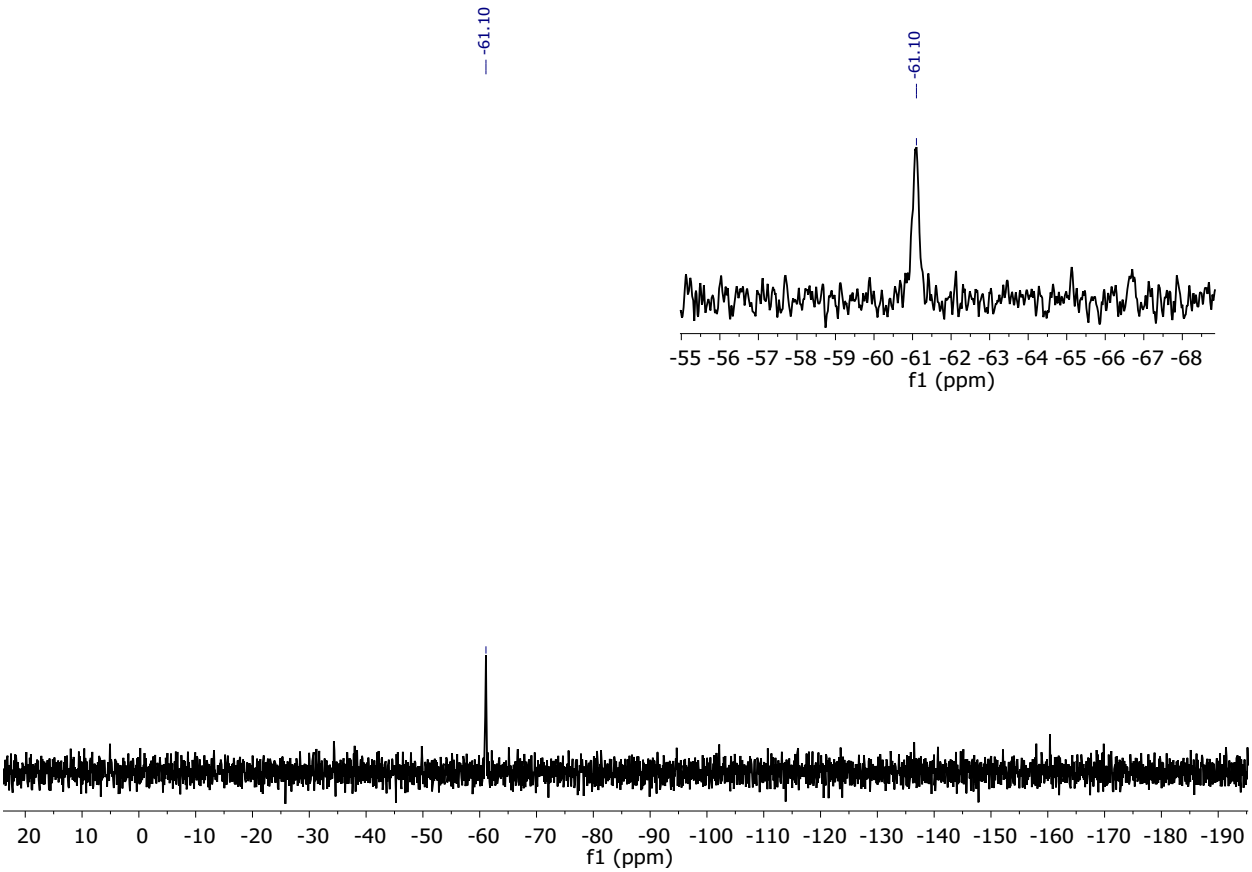

Figure S7. ^{19}F NMR spectrum of **2**-F in CD_2Cl_2.

Fluoride anion binding experiments monitored by $^{31}P\{^{1}H\}$ NMR spectroscopy using [2]BF_4 in the mixture of THF and water (8:2, v/v)

In a typical experiment, a KF (or KCl) stock solution in H_2O (5 M) was added by small increments (0.2 µL-30 µL) to an NMR tube containing an 8:2 THF/water solution (1 mL) of [**2**]BF_4 (5 mM). After mixing the solution by inverting the NMR tube upside down two times and by shaking it 5 times, the $^{31}P\{^{1}H\}$ NMR spectrum was recorded. The conversion to the corresponding fluoride adduct (**2**-F) was followed until the chemical shift of the signal no longer changed. The resulting data points were fitted to a 1:1 binding isotherm to provide the fluoride binding constant. No change in the $^{31}P\{^{1}H\}$ NMR was observed after addition of 50 eq. of KCl to [**2**]BF_4 indicating no appreciable formation of the chloride adduct.

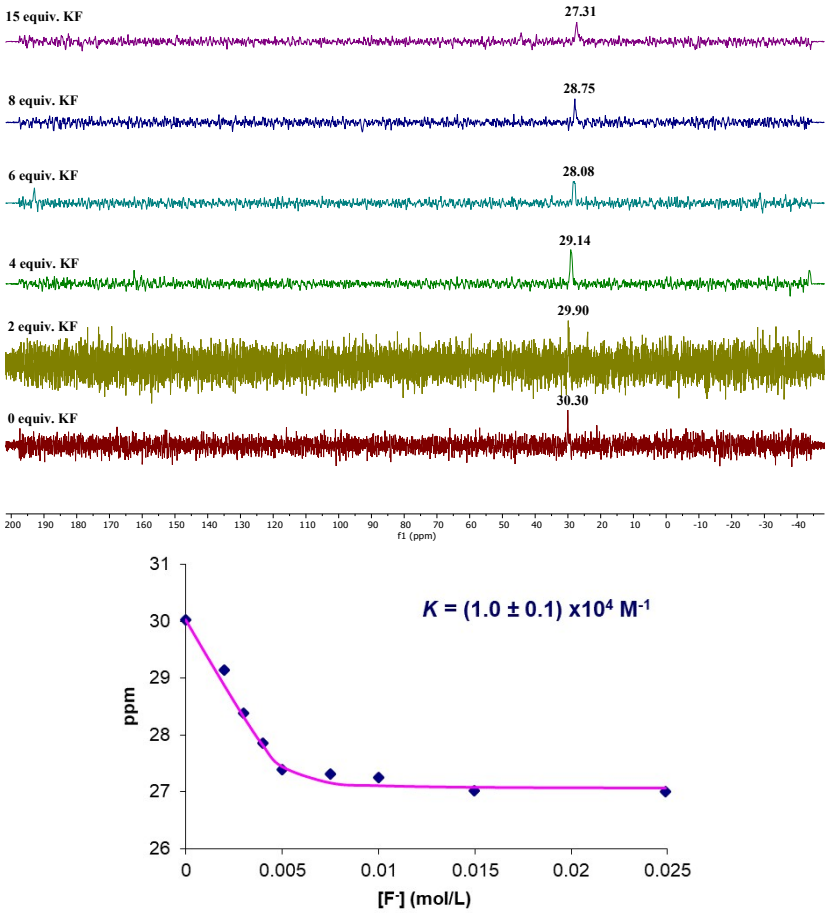

Figure S8. Top**:** Representative $^{31}P\{^{1}H\}$ NMR spectra obtained upon incremental addition of KF to [**2**]BF_4 in THF/H_2O 8:2 (v/v). Bottom: Resulting chemical shift data and 1:1 binding isotherm providing the best fit to the experimental data. This fitting afforded $K = (1.0 \pm 0.1) \times 10^4$ M^{-1}.

Computational details

All calculations were carried out using density functional theory (DFT) as implemented in the Gaussian 09 program.[8] All optimizations were conducted with the B3LYP[9] functional and mixed basis sets (cc-pVTZ[10] with ECP28 MDF[11] for Sb, 6-31+g(d) for P, 6-31g for all carbon, hydrogen and fluorine atoms) starting from the crystal structure geometries. No imaginary frequencies were found for the optimized structures, confirming that a local minimum on the potential energy hypersurface had in all cases been reached.

Table S1. XYZ coordinates of the optimized geometry of [**2**]$^{+}$.

Sb	-1.310260	0.023039	-0.063658	C	-1.265244	-3.089669	-3.158971
P	2.090840	0.101001	0.164594	H	-1.255861	-3.106692	-4.243600
O	0.924047	0.104344	-0.852709	C	2.666325	-2.408711	-0.858088
C	-1.289826	-1.840910	-1.080603	H	1.705559	-2.321005	-1.351835
C	1.254758	0.030610	1.777813	C	-1.568229	1.723955	-1.337306
C	-0.158719	0.005004	1.779908	C	-3.740342	1.107090	1.562198
C	4.927024	2.827806	-0.957455	H	-3.111792	1.985406	1.683179
H	5.728691	2.881198	-1.685833	C	-2.073980	3.904024	-3.028017
C	-3.281755	-0.009390	0.830988	H	-2.268072	4.748219	-3.681131
C	4.174206	1.656723	-0.839486	C	5.170605	-2.610769	0.393392
H	4.398556	0.808669	-1.477496	H	6.141374	-2.687505	0.870846
C	3.145601	-1.347404	-0.066342	C	-5.411108	-1.117068	1.249876
C	3.131327	1.577724	0.107982	H	-6.058486	-1.978433	1.122489
C	-0.128485	-0.160899	4.208209	C	-2.894074	2.102774	-1.624689
H	-0.669074	-0.238832	5.145294	H	-3.732434	1.566562	-1.197319
C	-0.756844	3.525737	-2.743188	C	3.440430	-3.562290	-1.018742
H	0.072713	4.073888	-3.177247	H	3.071267	-4.374822	-1.634868
C	-1.292717	-3.044558	-0.353762	C	-5.854094	-0.007960	1.977934
H	-1.301859	-3.041723	0.732139	H	-6.845303	-0.007579	2.418760
C	4.406737	-1.452160	0.555523	C	3.613574	3.858790	0.804314
H	4.801417	-0.631623	1.146180	H	3.399293	4.709922	1.441380
C	1.958820	-0.036881	2.991640	C	4.687578	-3.666003	-0.391845
H	3.043908	-0.021775	2.994000	H	5.285427	-4.562185	-0.518911
C	2.854054	2.691732	0.926566	C	-1.282300	-4.267518	-1.036884
H	2.055383	2.648027	1.658867	H	-1.285803	-5.196444	-0.476419
C	1.269404	-0.129574	4.204590	C	-0.496513	2.434859	-1.905724
H	1.819864	-0.181645	5.137387	H	0.521407	2.127658	-1.716663
C	-0.841000	-0.095855	3.003393	C	-5.017896	1.105597	2.132916
H	-1.923017	-0.125577	3.026925	H	-5.360474	1.970500	2.691495
C	-1.271924	-1.862200	-2.485307	C	-1.270748	-4.289915	-2.436885
H	-1.255503	-0.937895	-3.053110	H	-1.267763	-5.238476	-2.963220
C	4.649269	3.927426	-0.135437	C	-3.140414	3.188318	-2.473335
H	5.238401	4.833666	-0.226510	H	-4.163739	3.471265	-2.695678
C	-4.131256	-1.120209	0.678024				
H	-3.809255	-1.986883	0.111042				

Table S2. XYZ coordinates of the optimized geometry of **2**-F.

Sb	-1.208266	-0.176907	-0.020458	C	4.961072	-3.158767	0.588806
P	2.159235	-0.196431	-0.064863	H	5.980631	-3.242517	0.951117
F	-0.724126	-2.120781	-0.428617	C	-1.137482	4.310017	-0.192957
O	0.964255	-0.107762	0.906249	H	-0.935495	5.053567	-0.958813
C	3.036319	-1.781678	0.030280	C	-0.853834	-1.245139	2.940757
C	-1.324067	1.964101	0.464866	H	0.203619	-1.118284	2.752022
C	0.061698	0.099268	-1.807545	C	-1.655480	2.383436	1.766735
C	0.265972	0.355283	-4.225588	H	-1.856245	1.647095	2.537648
H	-0.206591	0.492003	-5.193632	C	-5.537935	-0.761297	-2.423089
C	-3.094393	-0.399185	-1.064824	H	-6.479621	-0.901384	-2.945617
C	2.259618	0.071458	-2.888402	C	3.751133	3.206646	1.520910
H	3.339755	-0.019633	-2.825085	H	3.441155	3.934559	2.263236
C	1.465963	0.006361	-1.729263	C	-1.468602	4.712549	1.106181
C	4.357507	-1.899669	0.500474	H	-1.525349	5.768708	1.352563
H	4.911852	-1.019719	0.805509	C	4.965258	3.365500	0.844236
C	-1.781793	-0.916926	1.937055	H	5.601890	4.217107	1.061851
C	-3.154237	-1.084062	2.195454	C	2.926074	-4.194626	-0.228512
H	-3.889336	-0.843412	1.434769	H	2.366223	-5.084324	-0.497105
C	3.318689	1.161209	0.278902	C	-5.208612	0.491972	-1.894449
C	2.313731	-2.942364	-0.324674	H	-5.893857	1.327429	-2.005092
H	1.274530	-2.863105	-0.632189	C	5.359642	2.425550	-0.116689
C	1.659463	0.249378	-4.136705	H	6.300687	2.546730	-0.643334
H	2.271425	0.301113	-5.031351	C	-3.435539	-1.657091	-1.600639
C	-3.993645	0.672574	-1.218621	H	-2.746325	-2.485653	-1.483371
H	-3.751745	1.649796	-0.812592	C	-1.725911	3.746226	2.085700
C	-3.591589	-1.571310	3.434629	H	-1.982148	4.050509	3.096567
H	-4.654834	-1.696708	3.617760	C	-2.662804	-1.898487	4.427840
C	2.927891	2.110468	1.241695	H	-3.000587	-2.278687	5.387417
H	1.981670	1.984241	1.755138	C	4.248809	-4.305004	0.219482
C	-0.524823	0.274164	-3.072914	H	4.718518	-5.281118	0.289924
H	-1.604042	0.333928	-3.162414	C	-4.649734	-1.834272	-2.274719
C	4.541939	1.327933	-0.400517	H	-4.902520	-2.808923	-2.682096
H	4.864623	0.605110	-1.142655	C	-1.295256	-1.734068	4.176816
C	-1.063147	2.946863	-0.508999	H	-0.568104	-1.987779	4.943046
H	-0.795029	2.655153	-1.519616				

Natural bond orbital (NBO) analysis

The optimized structures were also subjected to NBO analysis. The molecular orbitals and NBOs were visualized and plotted using the Avogadro program.[12]

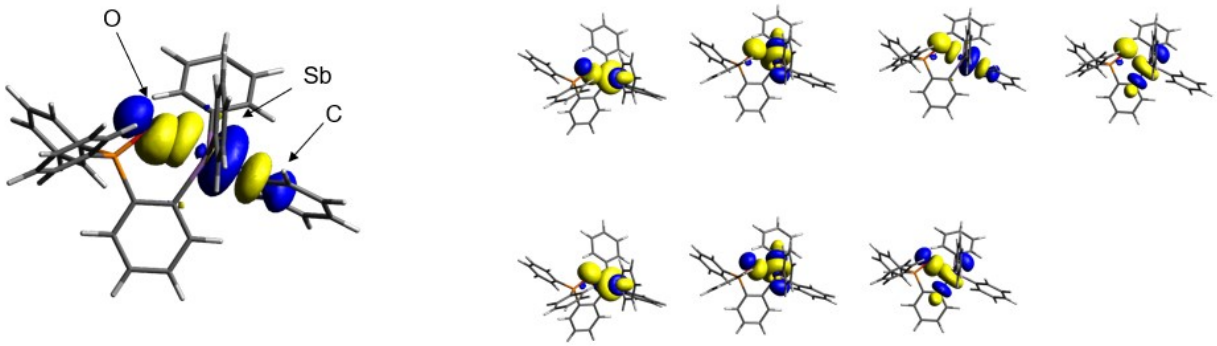

Figure S9. Donor-acceptor interactions (isovalue = 0.05) present in [**2**]BF_4. All lp(O) → σ*(Sb-C) donor-acceptor interactions contribute E_{del} = 51.9 kcal/mol to the stability of the compound.

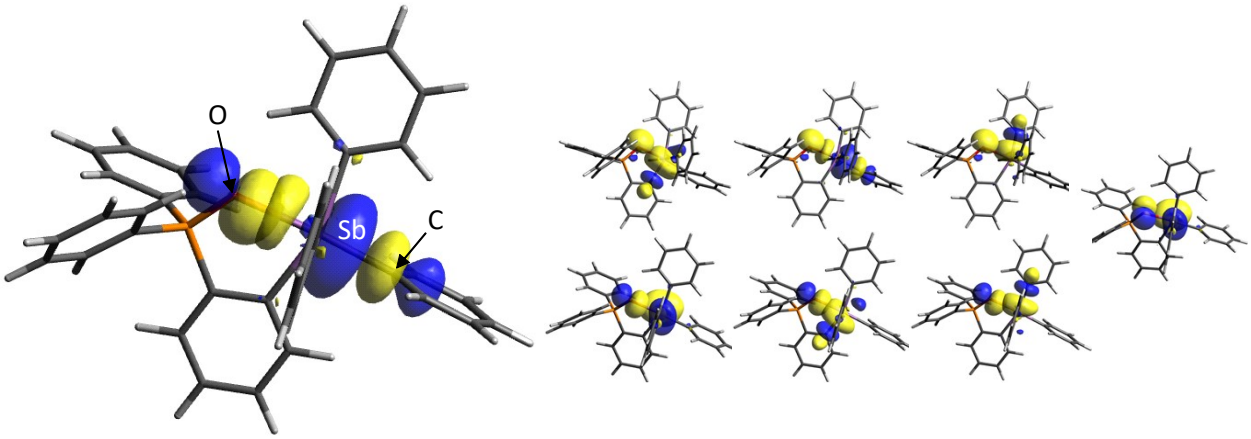

Figure S10. Donor-acceptor interactions (isovalue = 0.05) present in **2**-F. All lp(O) → σ*(Sb-C or Sb-F) donor-acceptor interactions contribute E_{del} = 55.7 kcal/mol to the stability of the compound.

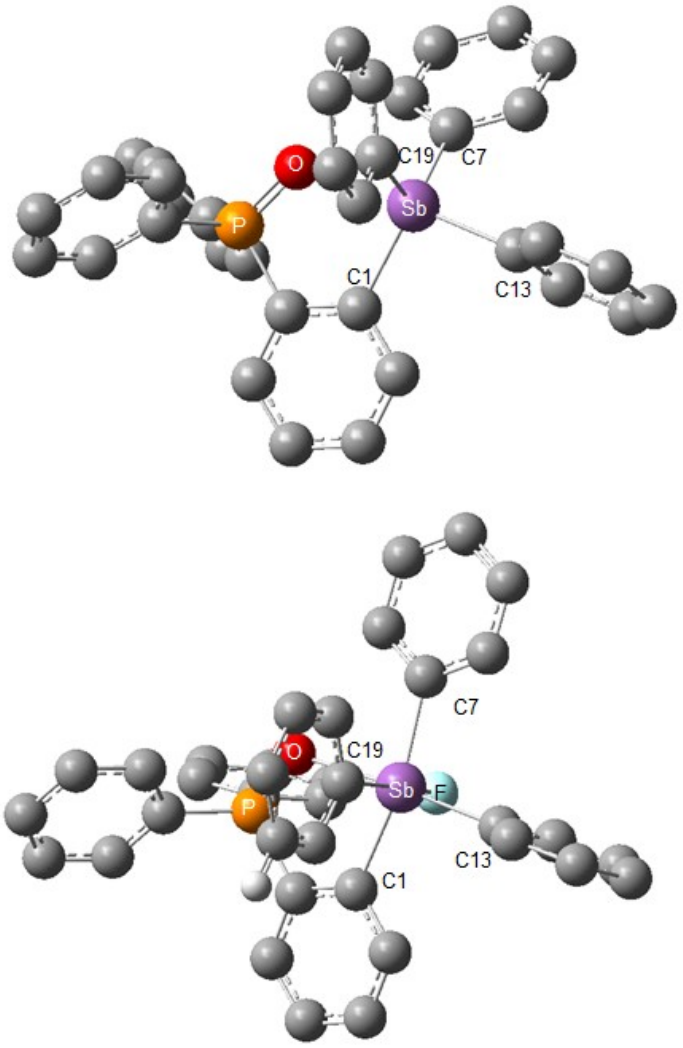

Bonding Orbital	Sb (%)	C (%)
Sb-C1	34.12	65.88
Sb-C7	36.98	63.02
Sb-C13	31.35	68.65
Sb-C19	35.08	64.92

Bonding Orbital	Sb (%)	C (%)
Sb-C1	29.94	70.06
Sb-C7	33.49	66.51
Sb-C13	29.37	70.63
Sb-C19	Fully ionic	

Figure S11. Parentages of the Sb-C bonding orbitals in [**2**][BF_4] (Top) and **2**-F (Bottom).

Electrostatic potential surface (ESPs) and distribution of the electrostatic potential on the molecular surfaces (V_S)

Electrostatic potential surfaces (ESPs) were created based on the optimized structures and determined at an isodensity value of 0.001 electrons/Bohr.[13] ESP maps were generated and analyzed using the Mutliwfn program[14] and visualized using VMD.[15] The Mutliwfn program was also used to identify the positions of maximum electrostatic potential (V_S, max).

Fluoride anion affinity in the gas-phase (FIA)

All fluoride anion affinity calculations were carried out using density functional theory as implemented in the Gaussian 09 program.[8] The optimized geometries of [**2**]$^+$ and **2**-F were subjected to a single-point energy calculation using the gradient-corrected Becke exchange functional and the Lee−Yang−Parr correlation functional (B3LYP) with a mixed basis set (the cc-pVTZ[10] with ECP28 MDF[11] for Sb; 6-311+g(2d,p) for all C, H, F, and P). The reaction enthalpies ΔH were derived from the energy of each molecule (from the single-point calculation) corrected to enthalpy by the "thermal correction to enthalpy term" obtained in the frequency calculations. This approach was previoulsy benchmarked against the experimentally determined fluoride anion affinity of CF_2O.[16]

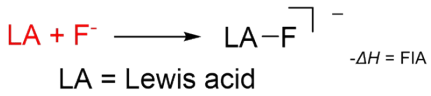

Partition Coefficients

Using a published approach[17, 18] illustrated in Figure S12, the solute electron density-based implicit solvation model (SMD)[19] was used to estimate the solvation of free energy of [**2**]BF_4 in water (ΔG_w) and in n-octanol (ΔG_o). Only the gas phase structure was optimized. The energy of the solvated molecule was obtained via single point calculations. The octanol-water partition coefficient K_{ow} was calculated based on the following equation with T = 298 K.[20]. The calculation results were determined to be: ΔG_w = -129.8217 kcal/mol , ΔG_o = -130.8128 kcal/mol, $-\Delta G_{ow}$ = 0.9911 kcal/mol, logK_{ow} = 7.20.

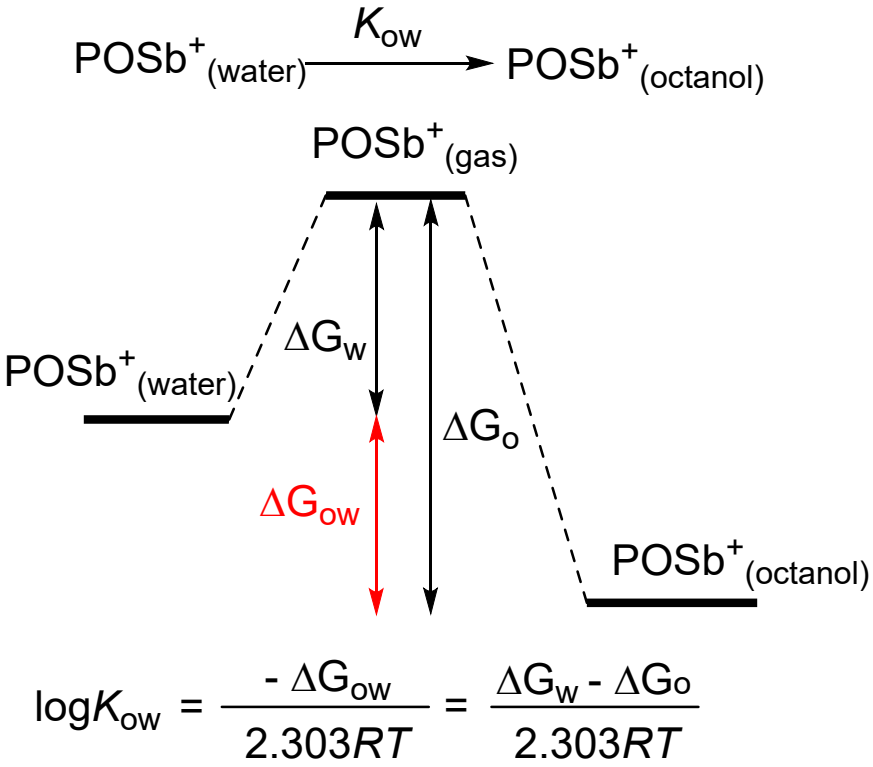

Figure S12. Diagram representing the approach adopted to determine the partition coefficient K_{ow}.

Vesicle preparation

POPC-LUVs. The transport experiments were conducted using POPC large unilamellar vesicles (200 nm diameter) loaded with a fluoride cargo. The vesicles were prepared according to a previously established method.[21] A thin film of the lipid was prepared by evaporation of a solution of POPC (40 mg) dissolved in $CHCl_3$ (1.6 mL). This film was dried under vacuum overnight. A buffered KF solution (1 mL, 10 mM HEPES, 300 mM KF, pH 7.2) was then added, resulting in a suspension which was then subjected to nine freeze-thaw cycles (liquid N_2, 47 °C water bath), and extruded 39 times through a 200 nm polycarbonate membrane. To remove any extravesicular component, the vesicle suspension was passed through a size exclusion column (Sephadex G-50) using a buffer solution (10 mM HEPES, 300 mM KGlc, pH 7.2) as an eluent.

Fluoride efflux in the presence of valinomycin

External solution: KGlc 300 mM, HEPES 10mM, pH 7.2

The following assay was adapted from a previous report.[22] POPC vesicles containing KF were suspended in the external solution (5 mL) such that the final lipid concentration was equal to 0.7 mM. After the electrode voltage had stabilized (~30 s), the measurement was initiated using a fluoride selective electrode. At t = 0 s, valinomycin dissolved in DMSO (0.7 mM) was added the assay such that the final valinomycin concentration was 0.1 mol %. At t = 30 s, aliquots of a 10 mM solution of the transporters ([**2**]BF_4 and [Ph_4Sb]OTF) dissolved in DMSO were added to the assay. At t = 300 s, 50 µL of a Triton X solution (10:1:1 H_2O:DMSO:Triton X (v/v/v)) was added to lyse the vesicles triggering complete release of the fluoride cargo. The value corresponding to 100% fluoride efflux was recorded at t = 420 s, 2 min. after lysing the vesicles. The data shown in the manuscript main text was replotted with t = 0 corresponding to the addition of the transporter. On this corrected scale, Triton-X 100 was added at t = 270s.

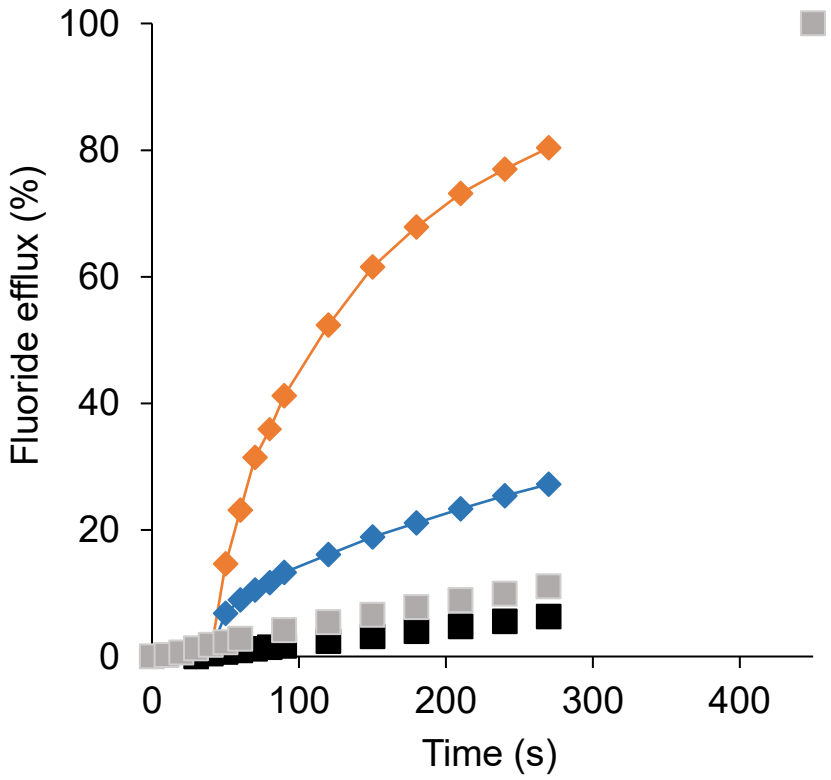

Figure S13. Fluoride efflux graph triggered by addition of 7 µL of 10 mM [**2**]BF_4 and [Ph_4Sb]OTf in DMSO solution.

Initial rate of fluoride efflux in the presence of valinomycin

---

The initial rate of fluoride efflux ($k_{ini.}$) was obtained by nonlinear fitting analysis of the experimentally measured fluoride efflux (%) versus time (s), with the following asymptotic function[23] using Origin Student 2020b:

$$y = a - b \cdot c(x-30)$$

y is the fluoride efflux (%)
x is time (s).
$k_{ini.}$ is then derived from $k_{ini.} = -b \cdot \ln(c)$ ($\% \cdot s^{-1}$).

The data points before the addition of transporters were omitted from the fit. Since the addition of transporters occurs at t = 30 s, we modified the function above.

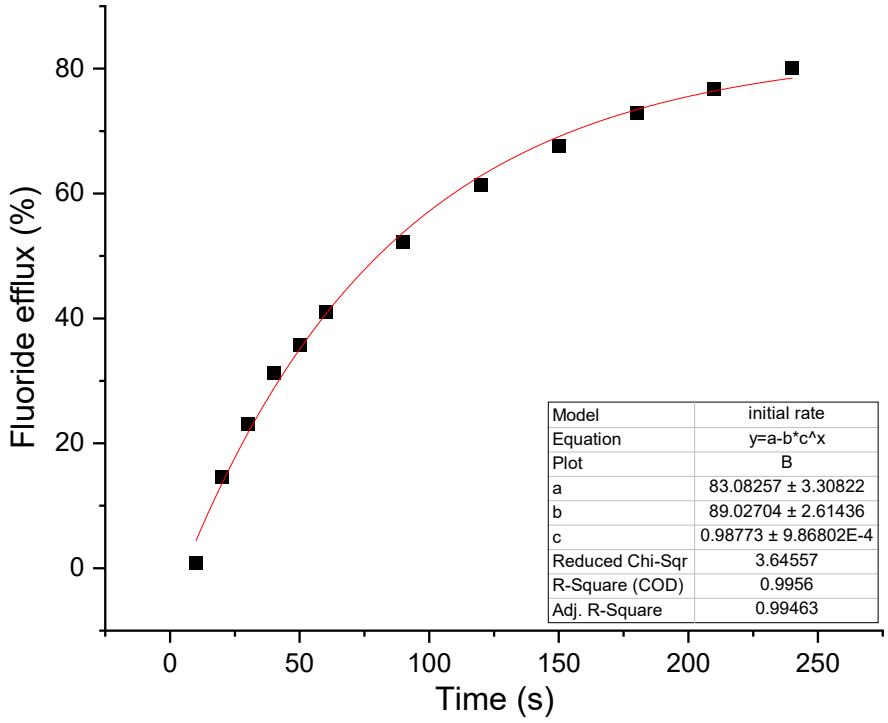

Figure S14. Kinetic fit of the valinomycin-coupled fluoride efflux data observed when POPC vesicles are treated with [**2**]BF_4 as a transporter (2.0 mol% with respect to the lipid concentration). The POPC vesicles were loaded with KF (300 mM) and suspended in KGlc (300 mM) buffered to pH 7.2. Each data point represents the average of two repeat measurements. $k_{ini.}$ = -b·ln(c) = 1.10 %·s^{-1}.

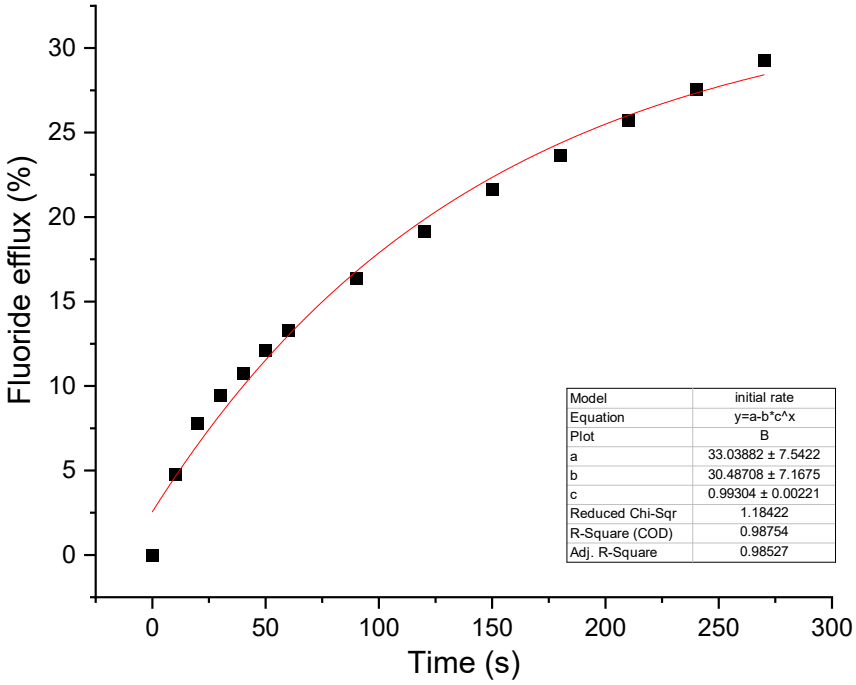

Figure S15. Kinetic fit of the valinomycin-coupled fluoride efflux data observed when POPC vesicles are treated with $[Ph_4Sb]OTf$ as a transporter (2.0 mol% with respect to the lipid concentration). The POPC vesicles were loaded with KF (300 mM) and suspended in KGlc (300 mM) buffered to pH 7.2. Each data point represents the average of two repeat measurements. $k_{ini.} = -b \cdot \ln(c) = 0.21\ \% \cdot s^{-1}$.

Hill plot measurement and analysis

The fluoride efflux assay described above was carried out with different concentrations of [**2**]BF_4. The resulting data was used to generate a Hill plot according to the following equation:

$$y = 100 \frac{x^n}{k^n + x^n}$$

where
x is the [**2**]BF_4 cation concentration
y is the fluoride efflux (%) at 270 s
n is the Hill coefficient
k is the EC_{50}.

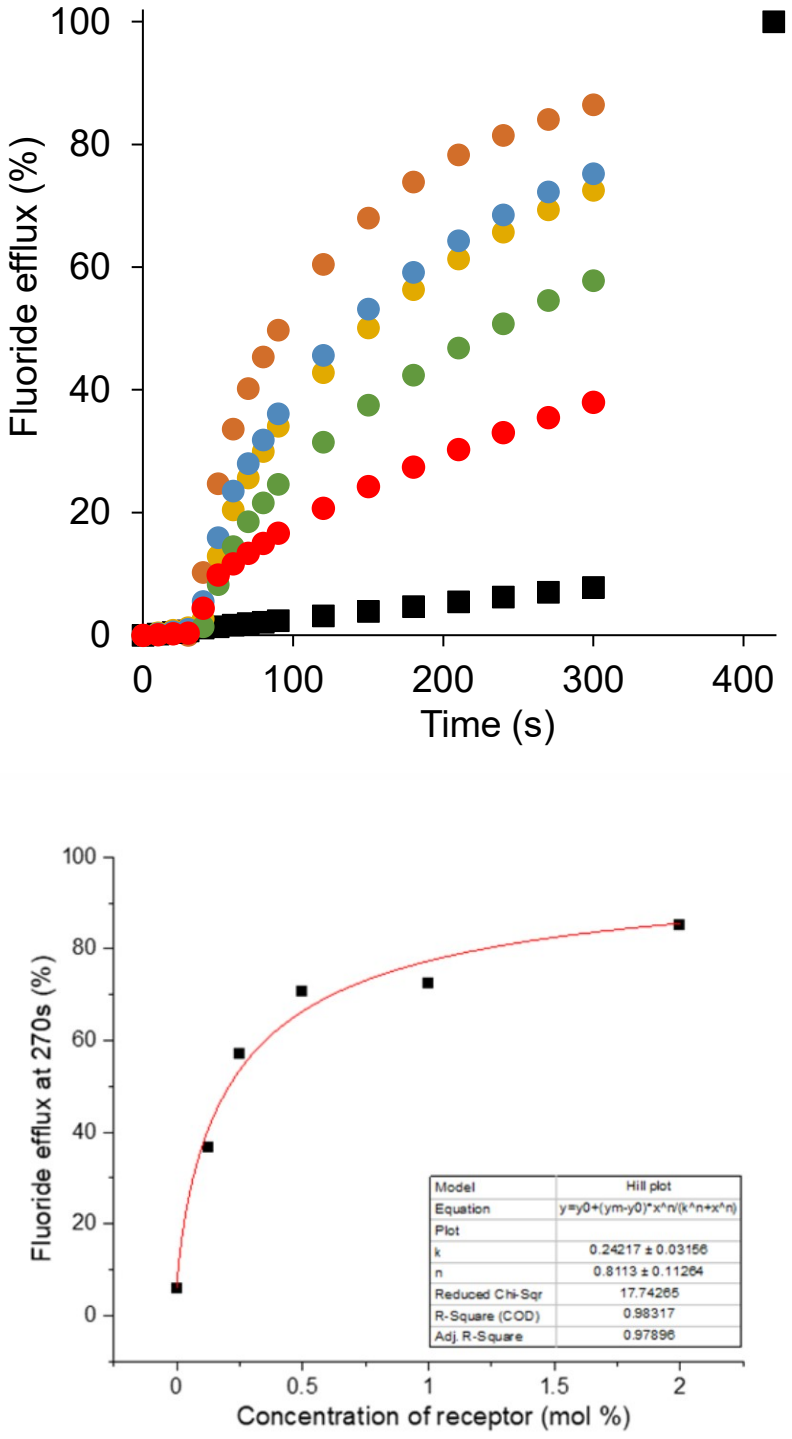

Figure S16. Hill plot analysis of the fluoride efflux from POPC vesicles (POPC concentration = 0.7 mM) mediated by [**2**]BF_4 in the presence of valinomycin. Valinomycin (0.1 mol% with respect to the lipid concentration) was added at time t = 0 s as a DMSO solution. After the 30 s, the transporter ([**2**]BF_4) was added as a DMSO solution, and the chloride efflux was monitored using a chloride selective electrode. At t = 300 s, 50 μL of a Triton X solution (10:1:1 H_2O:DMSO:Triton

X (v/v/v)) was added to lyse the vesicles triggering complete release of the chloride cargo. The value corresponding to 100% chloride efflux was recorded at t = 420 s, 2 min. after lysing the vesicles. For the graphs, the addition of transporter was set to t=0 s. Concentrations of [**2**]BF_4 used: 0 mol% (DMSO), 0.125 mol%, 0.25 mol%, 0.5 mol %, 1 mol%, 2 mol% with respect to the lipid concentration. (EC_{50} = 0.24 (±0.03) mol%, n = 0.81)).

Supplemental References

1. M. X. Yang, M. Hirai and F. P. Gabbai, *Dalton Trans.*, 2019, **48**, 6685-6689.
2. A. P. M. Robertson, S. S. Chitnis, H. A. Jenkins, R. McDonald, M. J. Ferguson and N. Burford, *Chemistry – A European Journal*, 2015, **21**, 7902-7913.
3. Bruker, 2019, APEX3 (v2019.2011-2010), Bruker AXS Inc., Madison, Wisconsin, USA.
4. G. M. Sheldrick, *SADABS, Version 2007/4, Bruker Analytical X-ray Systems, Inc., Madison, Wisconsin, USA*, 2007.
5. G. M. Sheldrick, *Acta Crystallographica Section A*, 2015, **71**, 3-8.
6. G. M. Sheldrick, 2014.
7. O. V. Dolomanov, L. J. Bourhis, R. J. Gildea, J. A. K. Howard and H. Puschmann, *Journal of Applied Crystallography*, 2009, **42**, 339-341.
8. M. J. Frisch, G. W. Trucks, H. B. Schlegel, G. E. Scuseria, M. A. Robb, J. R. Cheeseman, G. Scalmani, V. Barone, B. Mennucci, G. A. Petersson, H. Nakatsuji, M. Caricato, X. Li, H. P. Hratchian, A. F. Izmaylov, J. Bloino, G. Zheng, J. L. Sonnenberg, M. Hada, M. Ehara, K. Toyota, R. Fukuda, J. Hasegawa, M. Ishida, T. Nakajima, Y. Honda, O. Kitao, H. Nakai, T. Vreven, J. Montgomery, J. A.; , J. E. Peralta, F. Ogliaro, M. Bearpark, J. J. Heyd, E. Brothers, K. N. Kudin, V. N. Staroverov, R. Kobayashi, J. Normand, K. Raghavachari, A. Rendell, J. C. Burant, S. S. Iyengar, J. Tomasi, M. Cossi, N. Rega, J. M. Millam, M. Klene, J. E. Knox, J. B. Cross, V. Bakken, C. Adamo, J. Jaramillo, R. Gomperts, R. E. Stratmann, O. Yazyev, A. J. Austin, R. Cammi, C. Pomelli, J. W. Ochterski, R. L. Martin, K. Morokuma, V. G. Zakrzewski, G. A. Voth, P. Salvador, J. J. Dannenberg, S. Dapprich, A. D. Daniels, Ö. Farkas, J. B. Foresman, J. V. Ortiz, J. Cioslowski and D. J. Fox, *Gaussian 09*, Revision D.01, Gaussian, Inc., Wallingford, CT, 2013.
9. P. J. Stephens, F. J. Devlin, C. F. Chabalowski and M. J. Frisch, *The Journal of Physical Chemistry*, 1994, **98**, 11623-11627.
10. A. D. Becke, *The Journal of Chemical Physics*, 1993, **98**, 5648-5652.
11. B. Metz, H. Stoll and M. Dolg, *Journal of Chemical Physics*, 2000, **113**, 2563-2569.
12. M. D. Hanwell, D. E. Curtis, D. C. Lonie, T. Vandermeersch, E. Zurek and G. R. Hutchison, *Journal of Cheminformatics*, 2012, **4**, 17.
13. N. Bricklebank, S. M. Godfrey, H. P. Lane, C. A. McAuliffe and R. G. Pritchard, *Journal of the Chemical Society, Dalton Transactions*, 1994, DOI: 10.1039/DT9940001759, 1759-1763.
14. T. Lu and F. Chen, *Journal of Molecular Graphics and Modelling*, 2012, **38**, 314-323.
15. W. Humphrey, A. Dalke and K. Schulten, *Journal of Molecular Graphics*, 1996, **14**, 33-38.
16. M. Melaïmi, S. Sole, C.-W. Chiu, H. Wang and F. P. Gabbaï, *Inorganic Chemistry*, 2006, **45**, 8136-8143.
17. R. F. Ribeiro, A. V. Marenich, C. J. Cramer and D. G. Truhlar, *Journal of Physical Chemistry B*, 2011, **115**, 14556-14562.
18. M. Kolar, J. Fanfrlik, M. Lepsik, F. Forti, F. J. Luque and P. Hobza, *Journal of Physical Chemistry B*, 2013, **117**, 5950-5962.

19. A. V. Marenich, C. J. Cramer and D. G. Truhlar, *Journal of Physical Chemistry B*, 2009, **113**, 6378-6396.
20. F. Vlahovic, S. Ivanovic, M. Zlatar and M. Gruden, *J Serb Chem Soc*, 2017, **82**, 1369-1378.
21. H. J. Clarke, E. N. Howe, X. Wu, F. Sommer, M. Yano, M. E. Light, S. Kubik and P. A. Gale, *Journal of the American Chemical Society*, 2016, **138**, 16515-16522.
22. H. J. Clarke, E. N. W. Howe, X. Wu, F. Sommer, M. Yano, M. E. Light, S. Kubik and P. A. Gale, *J. Am. Chem. Soc.*, 2016, **138**, 16515-16522.
23. L. A. Jowett, E. N. W. Howe, X. Wu, N. Busschaert and P. A. Gale, *Chem.-Eur. J.*, 2018, **24**, 10475-10487.